38th International Electric Vehicle Symposium and Exhibition (EVS38)
Göteborg, Sweden, June 15-18, 2025

Manufacturing analysis of a molded electric motor design with internal stator cooling

Christian Stemmler[1], Marcel Laux, Julian Kraft,
Martin Doppelbauer
[1]*Fraunhofer ICT, Joseph-von-Fraunhofer-Straße 7, 76327 Pfinztal, Germany*
christian.stemmler@ict.fraunhofer.de

Executive Summary

In this study, the overmolding process of an electric motor with internal stator cooling technology utilizing composite materials shall be investigated. A comprehensive concept has been developed for a high-performance continuous power traction motor featuring distributed hairpin winding. However, the limited design space, stator design with multiple materials as well as increased machine dimensions for a high-power electric motor create challenges in optimizing electromagnetic, thermal, and manufacturing designs. The technical feasibility in large scale production processes is particularly crucial for the industrialization of the presented concept. In this context, three test specimens with increasing complexity were designed and produced using transfer molding. This approach allows for the analysis of various aspects, including the effects of the production process and demolding, long-term durability, and the identification of design limitations of the concept.

Keywords: Electric Machine, Cooling, Packaging, Materials for EVs, Vehicle Manufacturing

1 Introduction

To achieve sustainable mobility, the development of efficient and lightweight electric drives is an important transformation step for the automotive industry. A key factor in this transition is the enhancement of both continuous power density and peak power availability in electric machines. By increasing power density, it becomes possible to reduce material usage through downsizing while maintaining the same power output, thus supporting resource-efficient design.

Previous studies have demonstrated that the use of composite materials in conjunction with overmolding technology offers significant potential for increasing power density in electric machines. This is achieved by implementing indirect internal slot cooling using water-glycol, which provides superior thermal management compared to conventional water jacket cooling systems [1]. Building on these findings, the PerKuel project advances these concepts through the development of a high-performance, resource-efficient composite electric motor. The target is a permanent magnet synchronous motor (PMSM) capable of delivering 390 kW of continuous power, with a continuous power density exceeding 6 kW/kg.

Thin-walled cooling channels, positioned between thermal hotspots and the cooling fluid, are fabricated using transfer molding to significantly enhance thermal performance. This is achieved by shortening thermal conduction paths, enabling a high slot filling ratio, and reducing the volume of overmolding material required [2]. This study investigates the manufacturing process of the composite overmolded motor concept in greater detail, with a focus on design and process parameters that support high power density, ensure process robustness, and maintain part quality for safe and reliable machine operation. Emphasis is placed on evaluating the feasibility of scaling the process for serial production.

2 Cooling Concept

2.1 Internal Cooling

An internal slot cooling channel, positioned within the overmolding beneath the innermost hairpin in each slot can significantly reduce winding temperatures. These thin-walled channels are formed by mold cores during the transfer molding process that encapsulates the stator and its windings. Compared to conventional water jacket cooling, this design minimizes the thermal path from the indirect water-glycol coolant to the windings, where the highest electrical losses occur. In the PerKuel motor design, thermal performance is further enhanced by incorporating an additional yoke cooling channel located between the stator slots, thereby maximizing the cooling potential for high-power applications. This design approach also eliminates the need for a large aluminum sleeve typically used for water jacket cooling. The concept, derived from coupled thermal and electromagnetic optimization, is detailed in [2]. Fig. 1 illustrates a rendering of the PerKuel motor with its composite housing and integrated internal water cooling, along with a performance comparison against a reference motor.

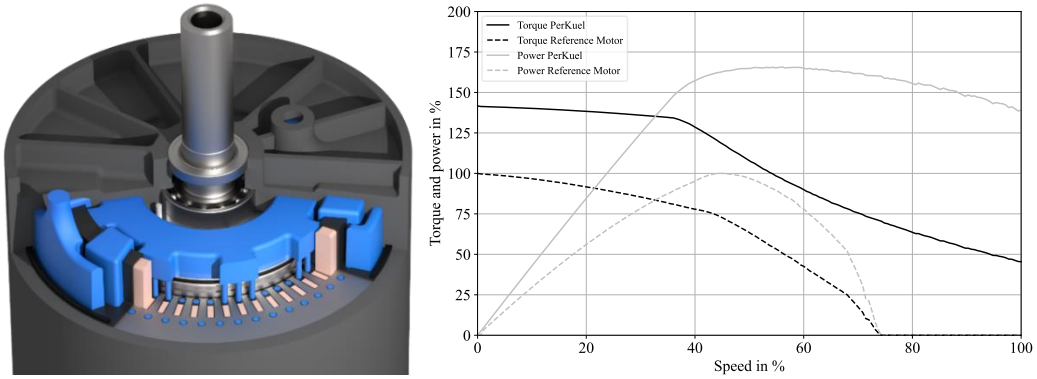

Figure 1: PerKuel design (left) and performance comparison between the PerKuel motor and the refence motor with state-of-the-art water jacket cooling (right)

The diagram in Fig. 1 (right) shows the percentage performance improvement of the PerKuel motor relative to a reference motor with aluminum housing for a water jacket cooling and no composite overmolding. Both designs were developed under identical system requirements, with design space constrained to the same longitudinal and radial dimensions. Additionally, the coolant flow rate and the maximum allowable pressure drop were kept constant. In the reference motor, the absence of internal cooling channels allowed for an increased number of hairpin conductors, thereby improving the slot filling ratio. The electromagnetic design was accordingly adapted to this configuration. Despite this, the reference motor exceeds the maximum permissible winding temperature significantly earlier across all operating points when compared to the PerKuel motor. This highlights the superior thermal management capability of the internal slot and yoke cooling concept. As a result, the PerKuel motor is capable of delivering 40 % more maximum continuous torque and sustaining operation at higher rotational speeds. Overall, this translates to a 65 % increase in maximum continuous power output.

2.2 Insulation Paper Substitution

To further improve cooling efficiency, the conventional low-thermal-conductivity insulation paper can be replaced with a higher thermal conductivity molded insulation layer. Previous studies have proposed a two-step molding approach: initially, the molded insulation layer is applied to the stator core, followed by the insertion of the winding coils. The complete stator assembly is then encapsulated in a subsequent transfer molding process [3].

Fig. 2 presents a cross-sectional view of an overmolded slot, highlighting the molded insulation layer (red) and conventional insulation paper (white) a colormap of the efficiency difference of both solutions. The substantial thermal improvement resulting from this insulation layer was systematically analyzed through a performance sensitivity study conducted for the PerKuel motor. At the operation point corresponding to the highest copper losses, this approach led to approximately 20 % reduction in maximum winding temperature relative to the coolant temperature, compared to the conventional insulation paper approach [2].

A cost-benefit analysis indicates that this method not only enhances thermal performance but also offers potential cost savings in serial production. Specifically, it eliminates the labor-intensive process of folding and inserting insulation paper into the slots, replacing it with a streamlined two-step stator molding process. Notably, significant thermal improvements can be achieved using a thermally conductive molded insulation layer alone, while the subsequent overmolding process - which accounts for roughly 90 % of the total composite material volume - can utilize a more cost-effective material with lower thermal conductivity.

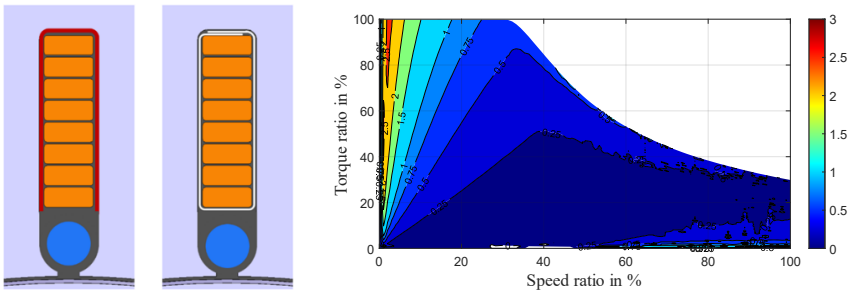

Figure 2: Insulation layer (red) and insulation paper (white) and colormap illustrating the efficiency difference of the insulation layer solution relative to the insulation paper dependent on torque and speed

Conversely, the diagram in Fig. 2 (right) illustrates the simulated efficiency difference between the molded insulation layer and conventional insulation paper as a function of torque and speed. For this comparison, the molded insulation layer was assumed to have a thickness of 0.4 mm, whereas the insulation paper was 0.2 mm thick. As a result, the use of the molded layer slightly reduced the slot filling ratio. In the medium torque and speed range, which is representative of the majority of operation time in typical drive cycles, a reduction in efficiency of approximately 0.15 % to 0.3 % was observed. This highlights an inherent design trade-off between increased continuous power enabled by improved thermal management and a slight reduction in overall motor efficiency. This study further investigates the manufacturability of the molded insulation layer, with a particular focus on minimizing its impact on efficiency through the use of thin-walled insulation designs.

3 Manufacturing Analysis

To investigate the feasibility of the production of the thin-walled structures in transfer molding, this study presents the analysis results of three test specimens, focusing on various aspects like general filling quality, interfacial strength between metal and plastic after lifetime equivalent preload, demolding effects on the mold or the overmolded electric motor. The test specimens are currently analyzed and will be completed in this study.

3.1 Interfacial strength metal – polymer & lifetime equivalent thermal preload

Strong adhesion between the epoxy molding compound and the over-molded stator lamination package is crucial to withstand loads by temperature cycles and vibration to achieve proper sealing against the conductive coolant and to prevent failure of the components by delamination and cracks, which applied especially for a directly cooled stator concept. In addition, the epoxy molding compound can only withstand high pull-out forces without delaminating or cracking, with sufficient adhesion to the stator lamination package. Cracks must be strictly avoided, as they may allow ingress of water-glycol mixtures, which could compromise electrically active components. Since the adhesive properties of the epoxy molding compound must be balanced to ensure proper mold release, mold release agents are added. As a result, sufficient adhesion to the stator lamination stack cannot be expected without appropriate surface modification. Therefore, various surface treatments and primer systems were investigated to identify reliable solutions such as a mesoporous SiO_2 adhesion film that is applied by microwave-induced plasma enhanced chemical vapor deposition and was initially developed for thermoplastic overmolding [4, 5], which deals as a benchmark due to extensive reference data. The two silane systems APTMS and GOPTS, were the APTMS was applied by dip-coating the specimens in a 0.5 % APTMS solution with butyl acetate as the solvent, which leaded to a film thickness of 1–2 µm. The GOPTS was applied undiluted with a fine brush and then dried at 75 °C for 2.5 h, leading to a film thickness of approx. 100 nm. The CILBOND® primer systems CB 48, CB 49SF and CB R-7222W, which were applied regarding their application data sheets [6, 7, 8]. The CB 48 primer was applied in two coats by a fine brush and air-dried. Film thickness was 15–40 µm. The CB49SF was also applied in two coats with a two-hour intermediate airing, then pre-baked at 100 °C for two hours, leading to a film thickness of 20–30 µm. The primer CB R-7222W was applied in two coats with two hours of intermediate ventilation, followed by two hours at 120 °C pre-baking, thickness 15–20 µm.

The substrate was made of a cold-rolled steel sheet according to DIN EN 1.0330, measuring 120 × 60 mm with a thickness of 1 mm. Before applying the pretreatment, all specimens were decreased with isopropanol and acetone. The samples were then over-molded with 2 mm of the epoxy molding compound Sumikon A730E via compression molding. To take the subsequent manufacturing and operating conditions into account as realistically as possible, all pretreatment methods were tested in three different configurations. At the first configuration the samples were placed in the mold at room temperature and then heated to 165 °C in the mold. The A730E material was heated to 90 °C in an external HF-preheater and then placed in the cavity above the substrate. Once the samples had reached mold temperature, the overmolding process was started. Heating took approx. 30-40 seconds, so that the pre-treatment did not undergo any thermal aging, and it was assumed that this would ensure maximum reactivity when overmolding with Sumikon A730E. To detect any thermal aging of the pre-treatments, the samples of the second configuration were preheated in a convection oven at 165 °C for two hours before overmolding, which reflects the subsequent production conditions when overmolding a stator. Due to the high mass, preheating the stator inside the mold is uneconomical and would increase the cycle time to a minimum of 20 min. In addition, a third configuration was used to investigate how thermal aging

affects the interfacial strength. The test specimens were cycled in thermal shock tests with a rapid aging profile for motor-related components in accordance with the VW 80000 standard [9]. The derived rapid aging profile was carried out at an amplitude temperature of +180 °C to -40 °C in a climate-conditioned elevator, for 100 cycles with a holding time of 15 minutes.

All specimens have then been mechanically tested using shear edge testing as described by Weidenmann et al. [10]. The rectangular specimens (8 × 10 mm) were extracted from the hybrid plates using waterjet cutting. Fig. 3 presents the measured interfacial strength in form of compression shear strengths and Figure 4 shows the corresponding fracture surfaces.

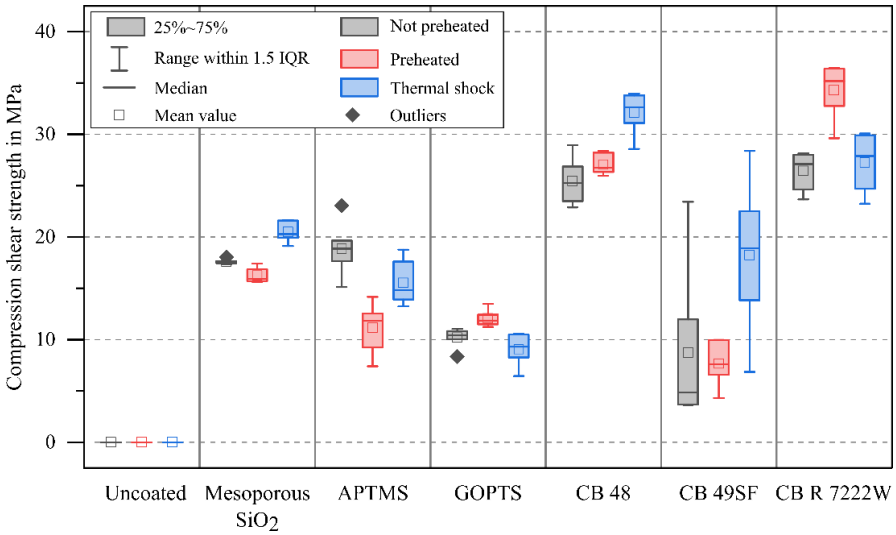

Figure 3: Compression shear strength of different pretreatment methods for the material Sumikon A730E on cold-rolled steel sheet (DIN EN 1.0330)

As expected, the untreated inserts showed no adhesion, and the fracture pattern shows no polymer residues at the metal surface.

The mesoporous SiO_2 film achieved up to 20 MPa with minimal variation between cold and hot insertions and retained adhesion after thermal shock. The fracture surface shows a thin layer of polymer evenly distributed across the metallic fracture surface. The fracture occurred at the SiO2-polymer interface. No significant differences between the cold-embedded and preheated samples could be detected. Only the thermal shock samples showed a slightly higher average adhesion. This could be related to post-crosslinking of the A730E during the first heating cycle of the samples to 180 °C.

APTMS showed high adhesion on non-preheated substrates with an average of 19 MPa, dropping by approx. 8 MPa after preheating yet still averaging 15 MPa after thermal cycling. GOPTS samples displayed lower adhesion (avg. 10 MPa), unaffected by preheating, and stable after thermal shock.

The highest interfacial strengths were observed with CB 48 and CB R-7222W, with average shear strengths of 25 MPa and up to 35 MPa for CB R-7222W after preheating. Both systems showed no degradation after thermal shock cycling. They also exhibited the least scattering in results, indicating consistent performance across samples. Specifically, CB 48 showed improvement after thermal shock cycling, suggesting reliability in maintaining adhesion strength under varying conditions. CB 48 even improved by ~7 MPa after shock cycling. The fracture pattern of both primer systems showed primary cohesive failure with a high amount of epoxy residues sticking to the metal surface.

CB49SF results were inconsistent. The average strength was 8 MPa, with significant scatter in non-preheated samples. After thermal cycling, values increased to an average of 19 MPa, possibly due to post-curing during the first cycle at 180 °C. The fracture pattern clearly showed cohesive failure of the CB 49SF primer. In combination with the large scatter, this primer appears less reliable for the application tested here.

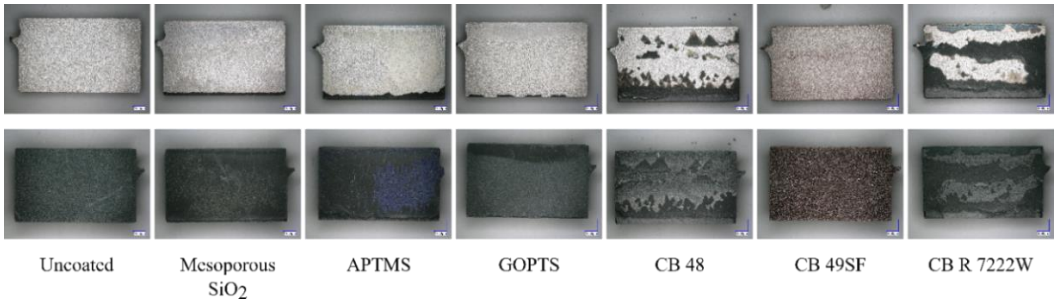

Figure 4: Fracture patterns with thermal cycling after mechanical testing with metal side (top) and polymer side (bottom)

3.2 Demolding effects - single slot - insulation layer

The insulation layer has great thermal potential for motor performance and cost-effective manufacturing. On the other hand, manufacturing thin-walled structures along extended lengths up to 200 mm, as well as the presence of great mold core geometries and a high slot count pose substantial challenges to the manufacturing process. The contact surface between the slot insulation layer core and the overmolded layer itself is considerably larger, compared to a round cooling channel within the slot or yoke. This increased surface area enhances specific adhesion, thereby raising the demolding force required to extract each core following the transfer molding process. To mitigate potential damage to the insulation layer, minimizing demolding forces is essential. Accordingly, a systematic investigation was conducted to evaluate demolding behavior as a function of core geometry and surface coating across multiple usage cycles.

To establish a robust and repeatable process while ensuring cost efficiency through reduced mold complexity and simplified test specimens, all experiments were conducted using single-slot lamination stacks subjected to overmolding. Specifically, 1 mm thick sheets of unalloyed steel grade 1.0330 according to DIN EN 10130, were laser-cut to incorporate multiple original slot geometries from the PerKuel stator design. These sheets were then stacked to lengths of 100 mm and 200 mm. Following stacking, the lamination assemblies were compacted and laser-welded at selected points that did not interfere with the slot overmolding region. Each assembled stack was subsequently wire-eroded to isolate individual slot test specimens. In accordance with findings from the previous chapter, all stator lamination stacks underwent surface pretreatment using CB R-7222W. The overmolding process was carried out using the advanced thermoset material Sumikon A730E.

The insulation layer cores were manufactured from 1.2343 steel according to DIN EN ISO 4957, a material commonly used for hot-work mold cores and ejector pins. The cores were milled to the required geometries, after which their surfaces were ground and polished in the direction of demolding to achieve a low surface roughness of Ra = 1.6 µm. Furthermore, the transition to the core head was designed to be free of notches to avoid stress concentrations that could lead to failure under high demolding forces. A representative test specimen, along with a corresponding core and the CAD model of the transfer molding tool, is shown in Fig. 5. The CAD model of the tool illustrates the test specimen with inserted core and the radial sprue gate at the inner diameter highlighted in yellow.

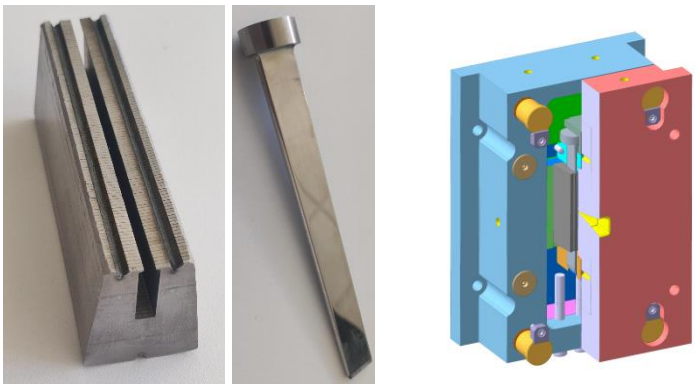

Figure 5: Slot test specimen and core for insulation layer molding (left) and transfer molding tool (right)

To investigate the influence of core geometry and surface coatings on the demolding process, each core was fabricated with distinct design features. Drawing from prior research and a market analysis of commercially available coatings suitable for thermoset composite transfer molding, two coatings were selected for evaluation: chromium nitride (CrN) and DICRONITE® DL-5, a modified tungsten disulfide (WS_2) in lamellar form [11, 12]. CrN was chosen for its exceptional wear resistance, making it particularly well-suited for use with abrasive thermoset materials and promoting extended tool life. In contrast, DICRONITE® DL-5 offers its extremely low coefficient of friction, which enhances resin flow and facilitates improved demolding, thereby contributing to higher part quality and reduced cycle times. The key properties of these coatings are summarized in Table 1.

Table 1: CrN and DICRONITE® DL-5 coating in comparison

	CrN	DICRONITE® DL-5
Hardness	2000-2400 HV	20-60 HV
Friction Coefficient (to steel)	0,3-0,57	0,03
Wear Resistance	excellent	good
Coating thickness	5 µm	0,5 µm

In addition to surface treatments, the impact of core geometry with and without demolding angles was investigated. In standard composite molding design, the application of a demolding angle is recommended to reduce demolding forces. However, in slot insulation molding for electric motors, introducing a demolding angle adversely affects electromagnetic performance by increasing the insulation wall thickness toward one end of the stator. This slightly reduces the motor efficiency, as detailed in Chapter Insulation Layer. To mitigate this negative effect, a subset of cores was ground at a slight angle, resulting in a wall thickness gradient from 0.3 mm at one end of the stator slot to 0.5 mm at the opposite end. For a stator with an active length of l = 100 mm, this corresponds to an angle of approximately 0.23°. For the longer 200 mm stator slots, the same wall thickness variation was maintained, resulting in a reduced demolding angle of 0.115°.

Furthermore, the influence of edge radius at the core-to-yoke transition was examined with respect to demolding behavior. A smaller edge radius allows for increased slot fill ratio but may also concentrate mechanical stress on a smaller contact area during demolding, potentially damaging the thin insulation layer. Two radii were evaluated in this study: $r_1 = 0.5$ mm, corresponding to the maximum wall thickness due to the demolding angle, and $r_2 = 1.2$ mm, which represents the largest radius permissible under electromagnetic constraints before significantly reducing the slot fill ratio. Fig. 6 (left) highlights the varied radius.

The majority of overmolding experiments were conducted using stator slots with an active length l = of 100 mm to systematically analyze various influencing parameters and enable direct comparison between test configurations. Subsequently, slots with l = 200 mm active length were overmolded to assess the scalability of the process for high-power applications, such as the PerKuel motor design. Fig. 6 (right) shows a single slot test specimen with molded insulation layer and molded edge protection.

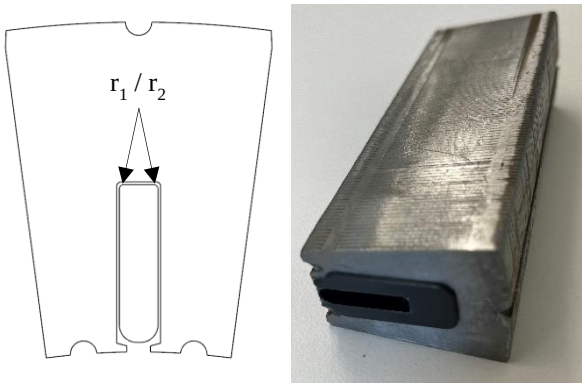

Figure 6: Drawing of a mold core inside of the slot highlighting the varied core radius (left) single slot test specimen with molded insulation layer and molded edge protection (right)

The majority of overmolding experiments were conducted using stator slots with an active length of 100 mm to systematically analyze various influencing parameters and enable direct comparison between test configurations. Subsequently, slots with a 200 mm active length were overmolded to assess the scalability of the process for high-power applications, such as the PerKuel motor design. During the molding process, all test specimens were preheated to a processing temperature of 170 °C and positioned in the main mold using a dedicated insert that also accommodated the insulation layer core. The thermoset composite material was injected through a radial film gate located at the inner diameter, positioned centrally along the slot length. Immediately after molding, while the components remained at elevated temperature, the inserts with the overmolded parts were extracted and transferred to a measurement apparatus for external core extraction, allowing for more precise determination of demolding forces.

In the context of potential large-scale production, three primary criteria were identified as critical for process viability. the maximum demolding force, which constrains the number of cores that can be simultaneously removed within the transfer molding machine and directly impacts cycle time and cost if external demolding is necessary. Then the overmolding quality, which is essential for ensuring long-term electrical insulation integrity and safety. Finally, the wear resistance of the cores, which dictates tool longevity and replacement frequency. To evaluate the influence of design and surface parameters on these criteria, each core configuration was subjected to three consecutive overmolding cycles. This allowed for assessment of run-in behavior and the evolution of demolding performance over repeated use. Fig. 7 presents a comparative overview of demolding force over displacement for the various test configurations, enabling detailed evaluation of the relevant influencing factors.

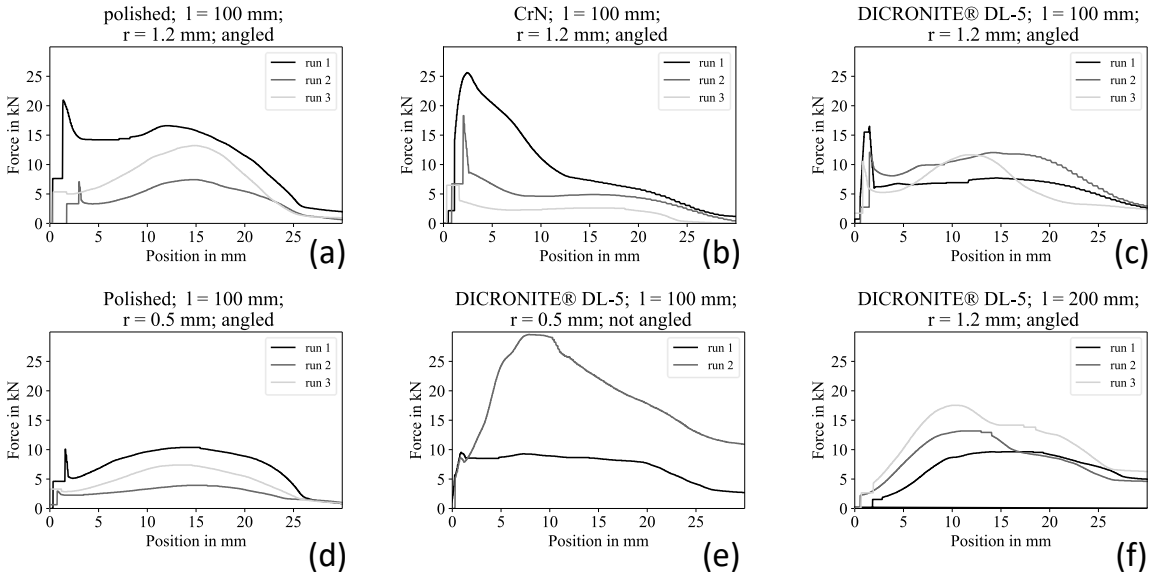

Figure 7: Force–distance diagrams for demolding tests with various core coatings and geometrical configuration

The diagrams (a), (b) and (c) show the demolding forces dependent on coating. The length of l = 100 mm, demolding angle and radius of r_2 = 1.2 mm were kept the same in these tests. The first run of native core (a), that was only polished, shows a peaking force of 21 kN after only a few millimeters. A high breakaway force is necessary to initiate sliding of the core. It then drops back to 15 kN before slowly rising to a local maximum of 17 kN located between 10 mm and 15 mm distance. After that, the force continues to fall to 2,5 kN with an increase of distance. In the second run the curve progression behaves similarly but with significantly reduced forces. The initial rise peaks at 7 kN and a second local maximum is reached at about 15 mm at a value of 7 kN. This corresponds to one third compared to the first demolding force. The force then continues falling to a low force of 2 kN at 30 mm. This development can be expected with the thermoset compound which contains a release agent that creates a remaining layer on the core surface during the processes. The third run shows no more initial peak and already starts to slide at a force of 5 kN. However, the force then rises high to a local maximum of 13 kN at about 15mm, more than twice as high in comparison to the second repetition, before falling to the low force of 2 kN. It was also noticed that the core had gotten clear signs of scratching during the third demolding.

To further investigate, all coatings were viewed with a scanning electron microscope before the first and after the last run shown in Fig. 8. The overmolding compound interlocking with the clearly visible scratches for the polished core caused by abrasive fillers in the thermoset compound explains the increase of demolding forces.

In the first demolding run, the CrN-coated core (b) exhibited the highest initial peak force among all tested configurations, reaching 25 kN. Unlike the uncoated variant, the force did not exhibit a distinct drop after the initial peak but instead followed a continuous decline, reaching approximately 2 kN at 30 mm of distance. Repeated runs resulted in a progressive reduction of both the breakaway and sliding forces. However, the overall force levels during core sliding were also notably lower in subsequent repetitions.

Microscopic analysis suggests that the high initial demolding force can be attributed to the inherent surface porosity of the CrN coating, which was observed in pre-test scanning electron microscope images. These micro voids likely increase the effective contact area and interlock with the thermoset material during the first cycle. After the first run, these pores appear to be partially filled or smoothed by the thermoset compound during molding, thereby improving the surface topography. This results in significantly lower demolding forces in subsequent runs. Furthermore, visual inspection with the scanning electron microscope revealed that the CrN coating experienced minimal visible wear or damage from the abrasive fillers in the thermoset compound. Due to its high hardness and wear resistance, CrN effectively protects the core surface, maintaining its structural integrity and surface properties over multiple demolding operations. Thus, while initial demolding resistance was high, the CrN coating demonstrated stable and repeatable performance after surface conditioning through initial use.

In the first run with DICRONITE® DL-5 (c) the property of a low friction coefficient can be seen clearly in comparison to the other coatings. A 25 % smaller starting peak is required to breakaway the core for sliding compared to the first polished core test. The curve then continues with a rather flat rise to only 7 kN at 15 mm before it falls to 2.5 kN in the end. The two following tests show decreasing peaks but a distinct rise of demolding force during sliding of the core. It is reasonable to assume that the low hardness and the thin coating thickness of DICRONITE® DL-5 are too susceptible to the overmolded composite material as the coating was quickly removed during the first test, so that the following runs are almost comparable to utilizing a polished core. The change in the general surface topography associated with the removal of the coating during the first runs is clearly visible in the scanning electron microscope images. Additionally abrasive residues responsible for scratches in the core are visible.

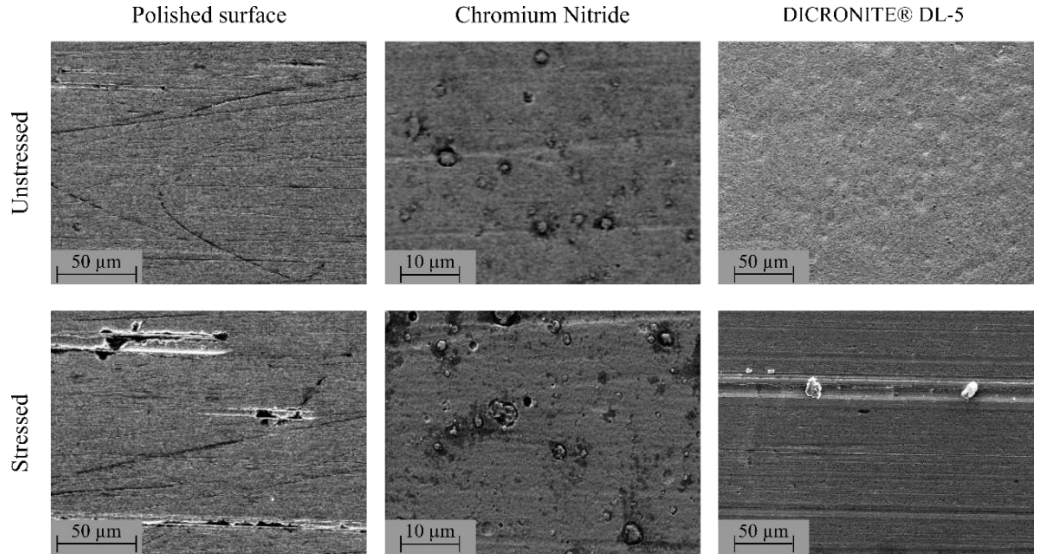

Figure 8: Scanning electron microscope images of each coating before the first and after the last run

Surprisingly, the radius also has a great influence on the demolding forces. A comparison between Fig. 7 (a) and (d) shows the force-distance diagram of two polished cores with different Radius. The demolding force of a core with the radius $r_1 = 0.5$ mm is reduced by factor 2 compared to a core with the radius $r_2 = 1.2$ mm. Despite the general curve progressions are similar, it is noticeable that the initial peak is not exceeding the second maximum anymore with the small radius. This improvement was measured for all coatings and is beneficial regarding the copper filling ratio in the slot.

As expected even though, diagram (e) in Fig. 7 has the small radius compared to diagram (c) a significant increase in demolding force was measured with a straight core compared to the angled one. The required demolding force to overcome the friction in the sliding phase is almost the height of the initial peak force, like in previous radius comparison. The first test shows a long plateau of about 1.5 times higher compared to the angled core. In the first repetition the forces then rise to an all-over extreme value of almost 30 kN, as the DICRONITE® DL-5 is already removed and damaged after the first test. In the second repetition the core even seized in the mold insert and no usable data could be generated. A closer look at the centering of the core shows worn composite material was pushed into small gaps during demolding and the core could not be removed.

Generally looking at the overmolded test specimen and the quality of the composite insulation layer it is important to summarize that with high forces and with increasing demolding force after multiple repetitions several frequently occurring damage patterns were determined. This was true for all combinations of coating, demolding angle and radius. Fig. 9 shows the images of the corresponding main damage patterns and the seized core (5).

The first image (1) shows damage of longitudinal cracks at the stator teeth, indicating that the interfacial strength was insufficient to withstand the applied demolding forces. As a result, the entire slot insulation layer detached from the stator, which significantly impairs thermal conductivity and poses a critical risk to long-term reliability. Image (2) displays material breakout in the same region, caused by localized tensile stress exceeding the composite's strength. Although such defects may theoretically be mitigated by a subsequent overmolding step for the cooling channels, the risk of propagating initial failures remains a concern.

In the third image (3) partial delamination is visible as fanning of the thin-walled insulation layer in the central region of the slot. To this, it must be considered that the demolding was done shortly after injection at almost process temperature of 170 °C, in alignment with short cycle times typical of serial production. At this stage, the composite material had not yet fully cured and retained a reduced mechanical strength. Further all shear edge tests in chapter 3.1 have been measured at room temperature, whereas demolding in the actual process occurs at elevated temperatures near the upper limit of the primer system's working range. This thermal condition may have compromised the mechanical integrity of the interface, contributing to delamination and compression-induced deformation. These observations reinforce the critical role of interfacial strength in the successful overmolding of stator insulation for electric drives. They also highlight the need to evaluate alternative primer systems with improved high-temperature stability.

Image (4) shows minor material wear in the lower corners of the slot base, where the radius was varied. This primarily occurred with the larger radius and under high demolding forces but was not considered critical with respect to the functional integrity of the insulation layer.

Figure 9: Damage Patterns (1)-(4) and seized core (5)

Nonetheless, in tests with decreasing force and particularly those without a pronounced initial peak the damage was greatly reduced, and full functional integrity of the insulation layer was maintained. Repeated overmolding cycles demonstrated that the release agent contained within the thermoset compound progressively reduces demolding forces, provided that the core surface remains intact. However, based on the prior results it was unlikely that successful demolding of cores with double the active length can be achieved without incurring critical damage to the insulation layer, regardless of core configuration.

As an approach to still achieve successful insulation layer at high length of l = 200 mm the additional polymer-based release agent LOCTITE® FREKOTE® HMT-2 was applied to the longer cores before the tests [13]. This release agent was selected due to its easy hot mold application with its fast-crosslinking properties for advanced composite molding. It is intended to reduce the initial high demolding forces during the first tests during the run-in phase until multiple processes have sufficiently applied the release agent contained in the composite material compound. The comparison of Fig. 7 (f) to (c) shows the potential of this final examination, where the length was doubled, and LOCTITE® FREKOTE® HMT-2 was applied. With this solution there is no more initial peak in demolding forces at all. During the first test an increase of 35 % to a maximum of 9.5 kN was measured. In the first repetition the same maximum of 12.5 kN is shown compared to the first test of the shorter slot. Only after that, with visible damage to the core, due to abrasive fillers, the demolding force again increased. Nonetheless, in all three tests a functional insulation layer resulted. These findings support the hypothesis that initial force peaks negatively affect overmolding quality and should be avoided. Notably, even a long, uncoated straight core could be successfully demolded using LOCTITE® FREKOTE® HMT-2, indicating that the release agent has a dominant influence compared to geometric parameters such as core radius, length, or demolding angle. However, to ensure long-term robustness, particularly against core abrasion, a protective coating remains important for potential serial production.

For a future research the next step will be a long-term focused analysis, combining the configuration of small edge radius, hard coating and additional mold release agent or also potential hybrid solutions of coatings for the first few runs and then to regularly examine the cores during a greater number of repetitions aiming to achieve robust manufacturing of straight insulation layers without demolding angle for maximal electromagnetic potential even at high active lengths.

3.3 Filling Study Motor Dummy segments

In addition to flat sheet specimens used for interfacial strength analysis and single-slot insulation layer tests, complex dummy motor segments were fabricated for preliminary evaluation of overmolding in realistic motor geometries. These segments consisted of welded 5 mm steel sheets featuring dummy winding heads and pre-inserted hairpins within the slots. A prior study examined the influence of molding compounds, wall thicknesses, and slot geometries on overmolding quality [2]. A CAD model illustrating the test specimens and the mold insert containing the round cores for the cooling channels is presented in Fig. 10.

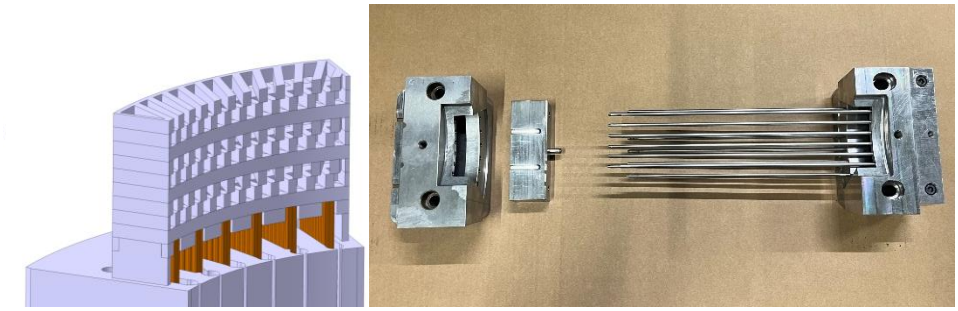

Figure 10: CAD model of a dummy motor segment (left) and mold insert with cooling channel cores (right)

3.3.1 Micrographs of overmolded motor dummy segments

For the motor design round cooling channel cores with a diameter of d = 4 mm achieve the best ratio of mechanical and electromagnetic design, cooling efficiency and pressure drop. Further, cooling channel diameters of d = 3.6 mm and d = 4.4 mm were tested to investigate the influence of wall thickness changes and potential bending of the cores due to different stiffness with different diameters. For this analysis the overmolded motor segments were cut into multiple cross sections over the active length of l = 220 mm and then compared to each other. Fig. 11 shows two micrographs of an exemplary overmolded dummy motor segment. As an indicator for comparison, the distance between the center of the channel diameter compared to the slot contour diameter was measured.

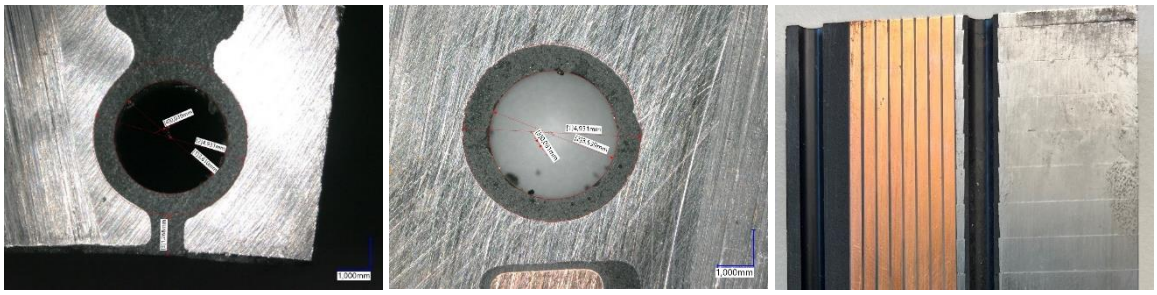

Figure 11: Micrograph of an overmolded dummy stator showing a slot channel (left) and a yoke channel (middle) and longitudinal section of both channels (right)

Generally, for these results, this distance was smaller than or equal to the production tolerance of 0.1 mm for the dummy segments. Furthermore, no tendency for oriented displacement or significant dependence on the core diameter was observed. This suggests that the influence of core bending during the transfer molding process is too small to be detected in this setup. Since the tests are based on the PerKuel motor concept, it was possible to demonstrate that core bending is not a critical factor for great motor dimensions. A more detailed analysis could be conducted in the future, using considerably thinner stator sheets to achieve better production tolerances or testing designs with even smaller channel diameters. On the other hand, it was clearly observed that the hairpins were displaced away from the cooling channel towards the yoke and were pressed against the stator. All hairpins were inserted at the center of the slot and were free to move radially. This effect is independent of the sprue position and can be explained by the lower flow resistance due to the increased wall thickness around the cooling channel, compared to the available space next to the hairpins. This effect prevents the hairpins from coming too close to, or entering, the cooling channels, which is beneficial for electrical safety. A simulation of the flow fronts will be discussed in the final chapter.

3.3.2 Process Simulation

During the analysis of the molded dummy motor segments, several challenges were identified in the filling process. For high-power motors with increased active length and stator diameter, a large shot volume must be injected in a short time before the gelation of the thermoset epoxy resin. Thin-walled cross-sections and the complex geometry of the wound stator result in varying flow resistances across different regions, potentially compromising the part's functionality by creating defects in the cooling channels if not properly filled. Fig. 12 illustrates entrapped air within a yoke cooling channel and a process simulation showing the flow fronts near the end of the filling process. The injection point, located at the top of the winding head, fills the dummy stator segment axially. This results in the top-side winding head filling first, with the material then splitting. While the majority of the material fills the slot, a smaller portion begins to fill the yoke channels. The flow resistance caused by the thin walls of the yoke channel delays its filling. The second winding head fills through the slot before the yoke channels are fully filled. The faster-moving flow front from the inner diameter then continues toward the yoke, reversing direction and trapping air within the yoke channel.

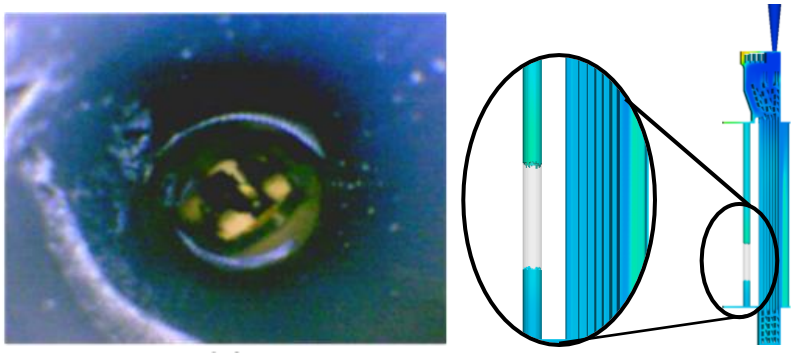

Figure 12: Endoscopy image showing entrapped air in a cooling channel (left) and image of a process simulation showing the position of the entrapped air (right) [2]

Proper analysis of the filling process is crucial for successful motor and mold design, particularly to prevent defects in the cooling channels. To optimize the filling process, several measures were considered. The primary goal was to prioritize the filling of the yoke channels before the rest of the motor was overmolded, with minimal impact on the electromagnetic and thermal design. Key influencing factors, such as flow resistance and sprue positioning, were adjusted.

Fig. 13 illustrates these modifications. Initially, a small restriction in the slot contour (A) was tested, filling unused space with stator sheet. This increased slot flow resistance but provided minimal improvement in the filling process. A thicker wall around the yoke channel (B) was also explored, either by increasing the stator hole size or reducing the cooling channel diameter. While a core diameter of d = 3 mm theoretically allowed proper filling without air entrapment, cooling efficiency decreased, and the pressure drop increased by 83 %, surpassing system requirements. Additionally, the sprue was moved to the outer diameter on top of the winding head (C), but this had little effect. A more complex solution involved relocating the sprue to the yoke channels (D), allowing the yoke to fill before the top winding head, thus reducing flow reversal into the yoke. However, without increasing the wall thickness of the yoke channels, this solution was insufficient. The flow resistance through the yoke channels is obviously the dominating factor.

Ultimately, improving the filling process through small geometric changes or sprue adjustments without affecting the motor design is challenging. A mold-only solution, such as incorporating a movable slider with a sealing ring in the bottom plate (E), could prevent composite material from flowing back into the yoke channel. The slider would seal the dividing passage during the main filling phase and open once the yoke channels are filled, which can be tracked with a sensor. This approach introduces additional mold complexity but given the relatively small impact on serial production costs, it warrants further investigation.

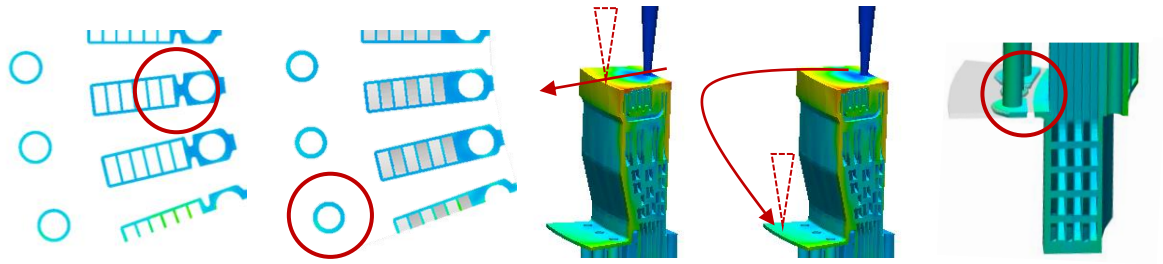

Figure 13: Process simulation modifications: flow restriction (A), increased wall thickness (B); sprue position on winding head (C) and yoke (D), mold sealing ring (E)

Conclusion

This study identified key factors in successfully manufacturing high-power molded electric motors with efficient internal cooling. The analysis shows that stator pretreatment for strong adhesion between thermoset material and metal surfaces is critical for mechanical integrity and long-term durability. Slot insulation molding offers major benefits, including improved thermal design and electrical safety, with a slight compromise in efficiency. Demolding tests confirmed the feasibility of molding functional slot insulation but emphasized that release agents or coatings are essential to reduce initial demolding forces, prevent core damage, and ensure process stability - especially during early cycles in potential serial production. Further challenges were found in filling stator geometries with many cooling channels, particularly isolated yoke channels. Variations in flow resistance and asymmetric slot layouts can cause air entrapment and compromise overmolding quality. While minor motor design changes yielded limited improvements, the study underscores the need for mold-focused solutions such as dynamic sealing elements and sliders.

Overall, this study opens new perspectives for the manufacturing of more powerful electric drives, whereby future research should focus on investigating the manufacturing processes with extended testing volume for long-term robustness of all materials used in serial production.

Acknowledgments

The PerKuel project is funded by the “Federal Ministry for Economic Affairs and Climate Action”. We extend our gratitude to all our partners involved in this interdisciplinary collaboration. We want to especially thank Sumitomo Bakelite Europe (Ghent) NV for the unwavering support by providing advanced composite materials and the dedicated contribution to manufacturing planning and execution. This publication was written within the framework of the KAMO: Karlsruhe Mobility High Performance Center (www.kamo.one).

References

[1] John, L.; Reuter, S.; Berg, L.-F.; Haehnlein, S.; Doppelbauer, M.; Resource-efficient integration of slot cooling channels in a hairpin electric motor. Elektromechanische Antriebssysteme 2023 - 9. Fachtagung (VDE OVE) Austria.

[2] Stemmler, C.; Laux, M.; Schröder, A.; Spanu, L.; Berg, L.; Doppelbauer, M.; Design and manufacturing limits of a thermoset composite overmolded electric traction motor implementing an internal cooling concept in a hairpin winding stator. 2024 14th International Electric Drives Production Conference (EDPC).

[3] S. Yamamoto, A. Nishikawa, T. Harada and W. Kosaka, Development of Direct Cooling Stator Structure Using High Thermal Conductive Epoxy Molding Compounds, 2022 International Power Electronics Conference (IPEC-Himeji 2022- ECCE Asia) Japan, IEEE, S. 407–414.

[4] Emmerich, R.; Dreher, R.; Urban, H.; Graf, M.; Bräuning.; Rüdiger.; Nauenburg, K.D. Nanoskalige Oberflächenstruktur zur Verbesserung der Adhäsion sowie Verfahren zu deren Herstellung, 2015.

[5] Laux, M.; Löhr, Y.; Dreher, R.; Emmerich, R.; Henning, F. Influence of the morphology of nanoporous silicon dioxide-based surface coatings on the interfacial strength of injection-moulded polymer-metal hybrids 2020, Hybrid 2020 page 200–205.

[6] Technical datasheet CILBOND® 48, https://www.icspecialties.com/de/produkte/haftvermittler/cilbond-48, accessed on 2025-04-28.

[7] Technical datasheet CILBOND® 49SF, https://www.icspecialties.com/de/produkte/haftvermittler/cilbond-49sf, accessed on 2025-04-28.

[8] Technical datasheet CILBOND® R-7222W, https://www.icspecialties.com/de/produkte/haftvermittler/Cilbond%20R-7222W, accessed on 2025-04-28

[9] ISO 16750-4:2023-07 Road vehicles - Environmental conditions and testing for electrical and electronic equipment - Part 4: Climatic loads.

[10] Weidenmann, K.; Pottmeyer, F.; Wang, Z.; Meiners, D.; Zinn, C.; Schaper, M.; Gonzalez, J. (2016). Shear edge tests: a benchmark in investigating the influence of different surface pretreatment methods on the shear stress of intrinsically manufactured metal-CFRP hybrids. International Journal of Automotive Composites. 2. 244. 10.1504/IJAUTOC.2016.10005303.

[11] Cunha, L.; Andritschky, M.; Pischow, K.; Wang, Z.; Zarychta, A.; Miranda, A.; Cunha, A. Performance of chromium nitride based coatings under plastic processing conditions. 2000 Surface and Coatings Technology. 133, 61-67.

[12] http://www.dicronite.de/produkte/dicroniter-dl-5.html accessed on 2025-04-28.

[13] https://www.henkel-adhesives.com/be/en/product/mold-release-agents/loctite_frekote_hmt-2.html accesed on 2025-04-28

Presenter Biography

Christian Stemmler graduated in mechanical engineering at the Karlsruhe Institute of Technology in 2020. His current research focuses on the development of high-power density electric drives using composite materials for lightweight design, implementing highly efficient cooling concepts, and increasing functional integration at the Fraunhofer Institute for Chemical Technology ICT in Karlsruhe, Germany.